Journal of Power Sources 246 (2014) 876–886

Contents lists available at ScienceDirect

Journal of Power Sources

journal homepage: www.elsevier.com/locate/jpowsour

A new open computational framework for highly-resolved coupled three-dimensional multiphysics simulations of Li-ion cells☆

Srikanth Allu*, Sergiy Kalnaus, Wael Elwasif, Srdjan Simunovic, John A. Turner, Sreekanth Pannala

Computer Science and Mathematics Division, Oak Ridge National Laboratory, Oak Ridge, TN 37831, USA

HIGHLIGHTS

- A framework for coupled models to simulate multiphysics phenomena of lithium ion battery.
- Importance of heat dissipation via metal current collectors is shown for cell configurations.
- The validation of the modeling approach by comparison with experimental results.

ARTICLE INFO

Article history:
Received 3 June 2013
Received in revised form
8 July 2013
Accepted 16 August 2013
Available online 24 August 2013

Keywords:
Lithium ion battery
Modeling
Computational framework
Multiphysics simulations

ABSTRACT

In this paper we report on the development and demonstration of physically consistent three-dimensional models for Lithium Ion Battery (LIB) cells. The discharge behavior of a LIB is a multi-physics and multiscale problem that is simulated using coupled models for thermal, electrical, and electrochemical phenomena. The individual physics models and software are integrated into a new open computational framework for battery simulations which was designed to support a variety of modeling formulations and computer codes. Several cell configurations (unrolled cell, unrolled cell with current collectors, large capacity pouch cell, and cylindrical cell) that show the importance of coupled simulations are simulated using this approach and discussed. A validation study is presented for the pouch cell discharged under high rates to demonstrate the accuracy of the proposed modeling framework.

1. Introduction

High energy density lithium-ion batteries are the primary power source choice for electric vehicles and large-scale military and space applications [1]. During various abuse conditions, overheating and uneven cooling of the battery and battery pack can result in rapid degradation and in extreme cases, uncontrolled electro-thermo-chemical reaction. High-performance battery packs or cells are designed to best perform within narrow temperature ranges. Mathematical modeling of battery thermal behavior and cooling strategies has proven to be an efficient and cost effective design tool for predicting life cycle issues and failure modes [2,3]. In order to make accurate life predictions, to improve performance and extend durability of the battery, the thermal variations within the electrode material must be taken into consideration. Approaches based on homogenization of the cell with averaged properties may not be appropriate when the thermal runaway and (or) electrical shorts need to be modeled due to lack of proper resolution of current collectors.

Several authors [4–6] have recently proposed coupling between the thermal models and representative electric circuit models for battery module. The coupling is implemented in two steps. First, an equivalent electric circuit is constructed to model the electric currents and overpotentials in the module. Then, the electrical solution is used to calculate the sources for the thermal equation. In the thermal model, the entire cell is homogenized based on volume averaged physical properties (e.g., thermal conductivity, thermal capacity, density)of the electrodes and current collectors. While being three-dimensional, such approach loses the spatial resolution of the currents in the collectors due to such circuit homogenization. In Ref. [7], authors propose a new 3D multiphysics model for Li-ion

☆ Notice: This manuscript has been authored by UT-Battelle, LLC under Contract No. DE-AC05-00OR22725 with the U.S. Department of Energy. The United States Government retains, and the publisher, by accepting this submission for publication, acknowledges that the United States Government retains, a nonexclusive, paid-up, irrevocable, worldwide license to publish or reproduce the published form of this submission, or allow others to do so, for United States Government purposes.

* Corresponding author. Tel.: +1 865 576 8784; fax: +1 865 241 0381.
E-mail address: allus@ornl.gov (S. Allu).

0378-7753/$ – see front matter © 2013 Elsevier B.V. All rights reserved.
http://dx.doi.org/10.1016/j.jpowsour.2013.08.040

battery, where the electric currents in collectors are modeled using two variables (one for positive current collector and the other one for negative). The currents are coupled with the electrochemical model via surface current density and the anisotropies in the connecting tabs are modeled using geometric relations.

In order to understand and predict the complex interplay between various coupled physics phenomena in Li-ion batteries, many electrochemical, thermal, and life models were developed [8–14]. Several codes [15–18] have been developed to bring these models under a single framework. However all these codes require the user to either rewrite or develop the model within the framework or to use the models that pre-exist in the code. Currently, there are no open-source computational platforms that can integrate these individual models beyond their original scope and application. Given the complex requirements for batteries for transportation applications, a predictive simulation capability which can guide design by considering performance and safety implications of different chemistry and materials choices is needed. We have developed an open computational framework that integrates the existing models that are independently developed and can also accommodate new models for simulating battery performance. The framework and the underlying models span across the cells, modules, battery pack, etc.

We are proposing an approach where electrochemistry, thermal and electrical transport are solved within a single simulation framework using three-dimensional representation. Multi-material interfaces are kept intact without homogenization assumption. A schematic for the cell sandwich model is shown in Fig. 1. Domains S and P represent cell sandwich (anode, separator, and cathode) and pouch material; PC and NC represent positive and negative current collectors. In Section 2, we describe the mathematical models for various physics and software components that are used in the framework for coupled simulation. In Section 3, we present the computing infrastructure and the underlying numerical methods for the framework. In Section 4, several battery simulation examples are presented to demonstrate the capability and accuracy of the approach.

2. Mathematical models

One of our main goals is to develop a modular framework so that individual components that correspond to particular physical phenomena can be flexibly and consistently interchanged with similar components. In this section, we describe the models for underlying physics phenomena, their mathematical formulations and computational implementations. The coupling between the models is discussed in Section 3.

2.1. Electrochemical models

Two models for electrochemical behavior were chosen in the present work. The first model takes experimentally measured polarization characteristics of the electrochemical cell as an input.

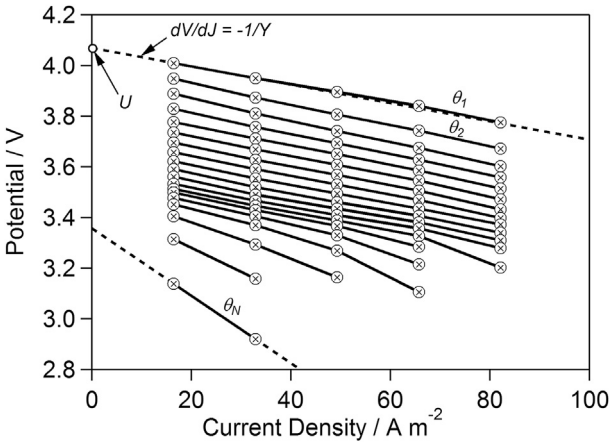

Fig. 2. Determination of the OCP and polarization parameter from the discharge data.

Linear dependency of discharge cell voltage on current density is given by Eq. (1) from Newman, Tiedemann [19] and Gu [20] for an electrochemical cell. This model is as also referred as NTG (Newman, Tiedemann, and Gu) model. The equations for the model are:

$$\begin{cases} J = Y\,(V_p - V_n - U) \\ U = \sum_{i=0}^{N} a_i \theta^i \\ Y = \sum_{i=0}^{M} b_i \theta^i \end{cases} \tag{1}$$

Variables Y and U represent effective conductance and open circuit potential of the cell as a function of depth of discharge (θ), and J is the current density transferred from the negative electrode to the positive electrode. Constants a_i and b_i are fitting parameters that are determined from cell discharge curves for a number of different C-rates. When the cell potentials are plotted against the current density coordinates, the intercepts of these curves at zero current density represent the values of open circuit potential U and the slopes represent the reciprocal of the cell polarization parameter Y. This is shown in Fig. 2, where the experimental data from the pouch cell discussed further in Section 4.3 is presented to aid the description of the method. Further details of the parameter calibration procedure can be found in Refs. [19,20]. The model Eq. (1) describes the overall characteristics of the cell without resolving local kinetics of electrochemical reactions or the internal concentration and potential gradients within the cell-sandwich. It is a linearized approximation of the full polarization curve. The NTG model has been widely used in cell and pack-level thermal modeling [3,21,22] due to simplicity of its implementation, provided the cell discharge curves are known for sufficient number of discharge rates.

The second implemented model for electrochemistry is based on the porous electrode theory [13,23–25]. The corresponding

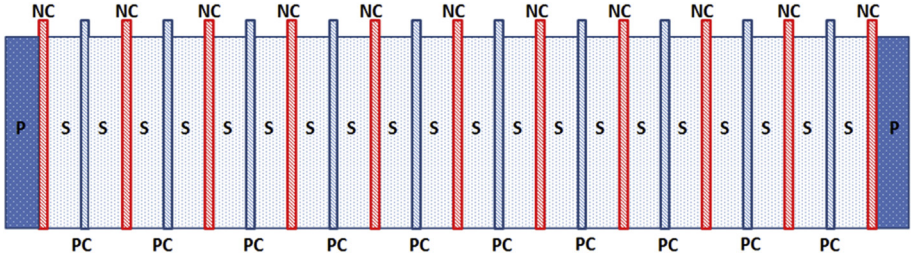

Fig. 1. Schematic of a Li-ion cell.

component within the framework is called *DualFoil*. The model employs one-dimensional description of the Li-ion transport from the negative electrode and into the positive electrode. Transport through the electrolyte is modeled by using the concentrated solution theory resulting in the equation for the lithium concentration (c_e) along the transversal direction z within the cell sandwich

$$\varepsilon \frac{\partial c_e}{\partial t} - \frac{\partial}{\partial z}\left(D_e^{\text{eff}} \frac{\partial c_e}{\partial z}\right) = a j_n \left(1 - t_+^0\right) \tag{2}$$

where ε is the volume fraction of electrolyte (assumed to be time-independent) and is equal to 1 in the separator region. D_e^{eff} is the effective diffusivity of lithium ion in the electrolyte, t_+^0 is the cation transference number, and j_n is the flux of Li^+ across the interface between the electrolyte and active electrode material. Obviously $j_n = 0$ in the separator region. The lithium flux is connected with the cell overpotential via the Butler–Volmer kinetics equation

$$j_n = \frac{i_0}{F}\left[\exp\left(\frac{\alpha_a F}{RT}\eta\right) - \exp\left(-\frac{\alpha_c F}{RT}\eta\right)\right] \tag{3}$$

where i_0 is the exchange current density, α_a, α_c are the anodic and cathodic transfer coefficients respectively, and η is the overpotential ($\eta_j = \phi_s - \phi_e - U_{(j,\text{OCP})}$). ϕ_e, ϕ_s represent the local potential of the electrolyte and the electrode material respectively, and $U_{j,OCP}$ is the open circuit potential for anode and cathode as a function of lithium concentration in solid phase (c_s).

The concentration of lithium in the solid phase (c_s) is determined by the diffusion equation

$$\frac{\partial c_s}{\partial t} - \frac{1}{r^2}\frac{\partial}{\partial r}\left(D_s^{\text{eff}} r^2 \frac{\partial c_s}{\partial r}\right) = 0 \tag{4}$$

with r being the radial coordinate of a representative spherical active material particle and D_s^{eff} representing the effective diffusivity. The above transport equations are complemented by the equations corresponding to the conservation of charge in electrolyte Eq. (5) and in active material Eq. (6)

$$\frac{\partial \phi_e}{\partial z} + \frac{2RT}{F}\left(t_+^0 - 1\right)\left(1 + \frac{\partial \ln f_A}{\partial \ln c_e}\right)\frac{\partial \ln c_e}{\partial z} + \frac{i_e}{k^{\text{eff}}} = 0 \tag{5}$$

$$\frac{\partial \phi_s}{\partial z} + \frac{i_s}{\sigma} = 0 \tag{6}$$

where f_A is the molar activity coefficient of the salt in the electrolyte. k^{eff} and σ represent respectively the ionic conductivity of the electrolyte and electronic conductivity of the solid active material. The second term in Eq. (5) represents contribution of polarization and obviously Eq. (5) reduces to Kirchhoff's law Eq. (6) for electrolytes with unity transference number. Influence of the transference number of electrolyte is discussed in detail in Ref. [26].

As can be seen, the entire electrochemical system can be cast into four conservation equations. Transport in electrolyte and electrode is given by Eqs. (2)–(4), and the conservation of charge is given by Eqs. (5) and (6). In this model it is assumed that the porosity of the electrode remains constant and that the volumetric strains resulting from lithium insertion are negligible. The details of the model derivation can be found in Refs. [13,23–25].

2.2. Thermal transport model

The transient three-dimensional heat conduction equation derived from the thermal energy conservation is:

$$\rho C_p \frac{\partial T}{\partial t} - \nabla(k\,\nabla T) = q \tag{7}$$

Where ρ is the density, C_p is the specific heat capacity, $k = \{k_x, k_y, k_z\}$ is the thermal conductivity, and T is local temperature. A general form of the heat generation term q in a battery has been derived by Bernardi et al. based on the energy balance within the cell [27]. The change in temperature within a battery cell is assumed to be caused by electrochemical reactions, changes in the heat capacity of the system, phase changes, mixing, electrical work, and heat transfer with the surroundings. Typically the heat of mixing and phase changes is ignored for the electrochemical systems [3,25,27–29], and the simplified form of the heat generation with addition of ohmic heating in the electrodes can be written as

$$q = \sum_j a_j i_j (\phi_s - \phi_e - U_j) + \sum_j a_j i_j T \frac{\partial U_j}{\partial T} + \sigma^{\text{eff}} \nabla\phi_s \cdot \nabla\phi_s + k^{\text{eff}} \nabla\phi_e \cdot \nabla\phi_e + \frac{2RT}{F}\left(1 - t_+^0\right)\left(1 + \frac{\partial \ln f_A}{\partial \ln c_e}\right)\nabla \ln c_e \cdot \nabla\phi_e \tag{8}$$

where the first term is the irreversible heat energy generated due to cell polarization, and the second term represents the reversible entropy change due to a reaction j. Quite often this latter entropic term is set to zero, either due to the lack of data describing the open circuit potential as a function of temperature [28] or based on the assumption of negligible influence on the total heat generation [30]. The rest of the terms in Eq. (8) represent the effect of ohmic heating in solid and electrolyte phases. The latter is typically ignored [21,22,28] so that the Eq. (8) simplifies to

$$q = \sum_j a_j i_j (\phi_s - \phi_e - U_j) + \sum_j a_j i_j T \frac{\partial U_j}{\partial T} + \frac{(i_s)^2}{\sigma^{\text{eff}}} \tag{9}$$

Eq. (9) is complemented by the sources due to ohmic heating in current collectors which are obtained from the electrical component (discussed in the next section).

When the NTG model is used within the electrochemical component, the heat source is represented as an integral quantity of the source in Eq. (8) in form

$$q = \left[J\left(\eta - T\frac{\partial U}{\partial T}\right) + \frac{J^2}{\sigma^{\text{eff}}}\right]\frac{1}{h} \tag{10}$$

where η is the cell overpotential ($V_p - V_n - U$), J is the current density passing through the cell (applied current normalized with respect to the total cell surface area), and h is the cell thickness. Such integral representation is because NTG model is based on homogenization across the entire cell and thus cannot resolve the internal profiles of the lithium concentration or electrolyte/electrode potentials.

The components of effective thermal conductivity in Eq. (7) are calculated taking into account the anisotropy of the thermal properties of the cell sandwich. With z-axis along the thickness of the cell sandwich, the transversal and longitudinal components of the effective thermal conductivity are calculated as

$$\begin{cases} k_z = \dfrac{\sum h_i}{\sum h_i/k_i} \\ k_x = k_y = \dfrac{\sum h_i k_i}{\sum h_i} \end{cases} \tag{11}$$

where h_i and k_i are the individual component thickness and thermal conductivities.

2.3. Electrical transport model

Electrical component within the framework is based on the Laplace's equation (equation for conservation of charge: Kirchhoff's law)

$$\nabla(\sigma \nabla V) = 0 \tag{12}$$

The effective cell sandwich conductivity (provided by the electrochemistry model in domain S of Fig. 1), and current collector conductivity (in domains NC and PC) is used when solving Laplace's equation on a single 3D domain with multi-material interfaces to maintain a consistent potential drop in the electrical simulation. For discharge behavior, a constant current is imposed as boundary condition on the edge of the current collector tabs.

Heat transfer equations and Laplace's equation for electronic transport are solved using the *Amperes*, a multiphysics 3D Finite Element (FE) code developed at ORNL. Given the different spatiotemporal scale of electrochemical and thermal transport, we undertake the simulations at respective scales using operator splitting method so that we have an efficient computational scheme to solve the coupled problem. The electrochemistry model requires a more refined discretization along the thickness of the cell compared to the thermal transport where a coarser discretization is sufficient.

The information between the different discretizations and models is exchanged by decomposing the cell domain into multiple zones along the various coordinate axes to account for the effect of temperature gradients on the electrochemical model. In each zone, an instance of electrochemical simulation is launched. The electrochemical solution provides the heat source for each of the zones. The *Amperes* component updates the temperatures for the each of the zones for the subsequent run of the electrochemical component.

3. Computational framework

The Open Architecture Software (OAS) framework for battery simulations was developed under the US Department of Energy research program Computer Aided Engineering for Batteries (CAEBAT). The framework is designed for transient simulations with relatively loose coupling between the various physics components. Each simulation component in the OAS framework is equipped with coupling interfaces that are implemented as python wrappers around standalone code executables. These interfaces convert native data from these executables to the data format used by the OAS framework. This enables the executables to remain unchanged and yet fully interact with the framework and other components. The OAS framework, the physics components, interfaces and the support tools, constitute the Virtual Integrated Battery Environment (VIBE).

With this framework, scientists and designers can utilize decades of effort that various communities have put into the development, verification, and validation of modeling tools for the individual physics domains, and focus on the new issues associated with coupling and multiphysics interaction. In many cases, the data exchanged by components is modest, and is easily managed through a battery state. The battery state is the minimal digital description of the battery in space and time such that each simulation component can apply their respective physics models and advance in time from one state point to the next.

The architecture of the OAS framework is shown in Fig. 3. The OAS framework is derived from the Integrated Plasma Simulator (IPS) developed by the Center for Simulation of RF Wave Interactions with Magneto-hydrodynamics (SWIM) [31]. The OAS is designed primarily for use in a batch processing environment, with a batch job typically comprising a single invocation of the framework, calling the individual physics codes underlying the components many times as the simulation progresses. OAS simulations are typically orchestrated by a "driver" component, though simulation-controlling logic can also be built into individual components. The OAS framework provides a set of services that are used by components within a simulation to facilitate the coupling process. The "framework services" communicates with the various physics based components through "component adapters." These components update the "battery state" through "state adapters." The detailed description of the functionality and services provided by the OAS framework can be found in Refs. [32,33].

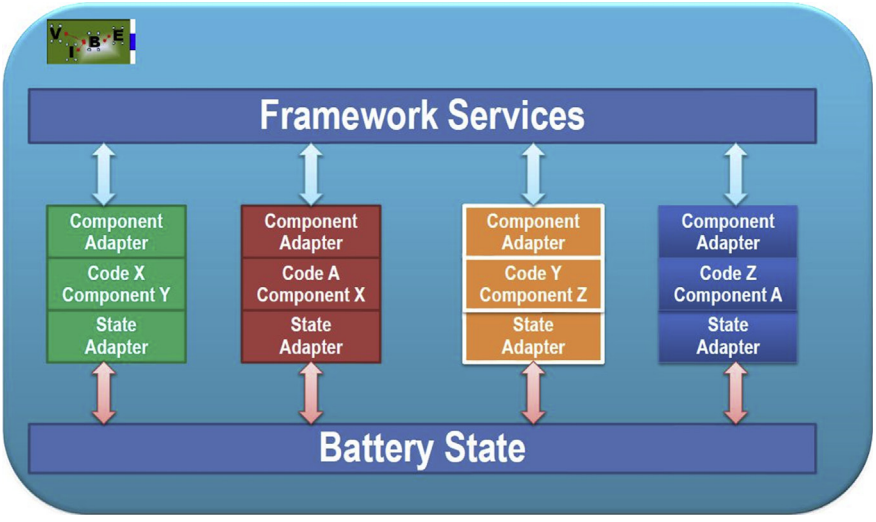

Fig. 3. Schematic of OAS framework.

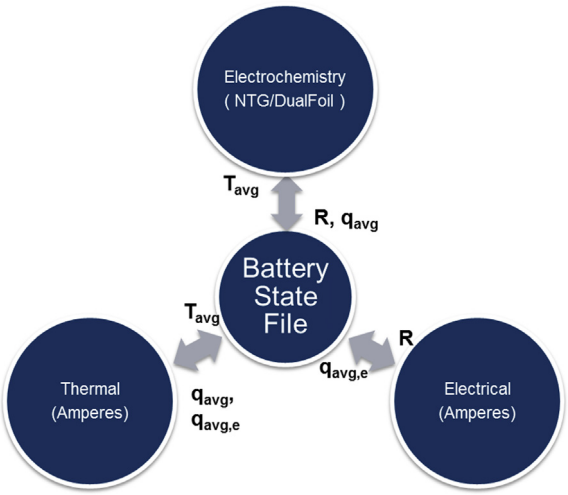

Fig. 4. Battery state.

The OAS framework supports multiple levels of concurrency, enabling efficient and flexible utilization of heterogeneous computational resources [32]. Individual physics based components can be serial or parallel, multiple instances of the component tasks can be executed concurrently in a simulation, and multiple simulations can also be run simultaneously. To demonstrate these features, we have implemented components into VIBE that support various levels of parallelism for modeling electrochemistry and mass, electron, and heat transport. The schematic of these components interacting with the battery state is illustrated in Fig. 4.

Based on the interaction of the dependent variables and the coupling, various computational strategies between these systems can be employed. When the influence between two states is predominantly in one direction, a one-way coupled numerical technique suffices to get plausible solutions. In a one-way or forward coupling, a set of variables in one of the physics components depends on the solution of the other components, but not vice versa. On the other hand, as the inter-dependence between the variables becomes strong a two-way coupled numerical technique must be used to obtain an accurate solution. In this case, the state variables within the components strongly depend on the solutions of the other components and exchange needs to occur in both directions. Picard iterative method is applicable to fully coupled physics, for example in cases when the interfaces or domains are shared between the two sets of physics. In the case of explicit coupling, the exchange of data between different physics occurs at the end of the time step, while the implicit coupling imposes simultaneous solution of all physics. Various coupling scenarios available for battery modeling are described in Fig. 5.

4. Numerical studies

To illustrate the flexibility of using various components under OAS framework and effect of choice of representative physics models, a series of three loosely coupled simulations of electrochemistry, electrical and thermal transport are discussed for several battery configurations. The developed framework was used to simulate multiphysics processes in typical battery cell configurations. The coupling between different physics solvers was implemented as a two-way loose coupling according to Fig. 5 and the number of interaction points between the two components has been varied to reach convergence. A validation study demonstrates a good fit between the experimentally measured temperature profile and the simulation. All the simulations were executed on 8 core AMD processor workstation with 8 GB memory.

4.1. Unrolled cell

In the first case study, we simulate the unrolled cell as described in Ref. [29]. Cell electrochemistry was modeled by *DualFoil* component. Two simulation scenarios were considered. In the first, *DualFoil* was coupled with thermal transport only. The second scenario couples *DualFoil* to thermal and electrical models.

The composition of the cell is identical to that described in Refs. [23,29]. Lithium manganese oxide was used as an active cathode

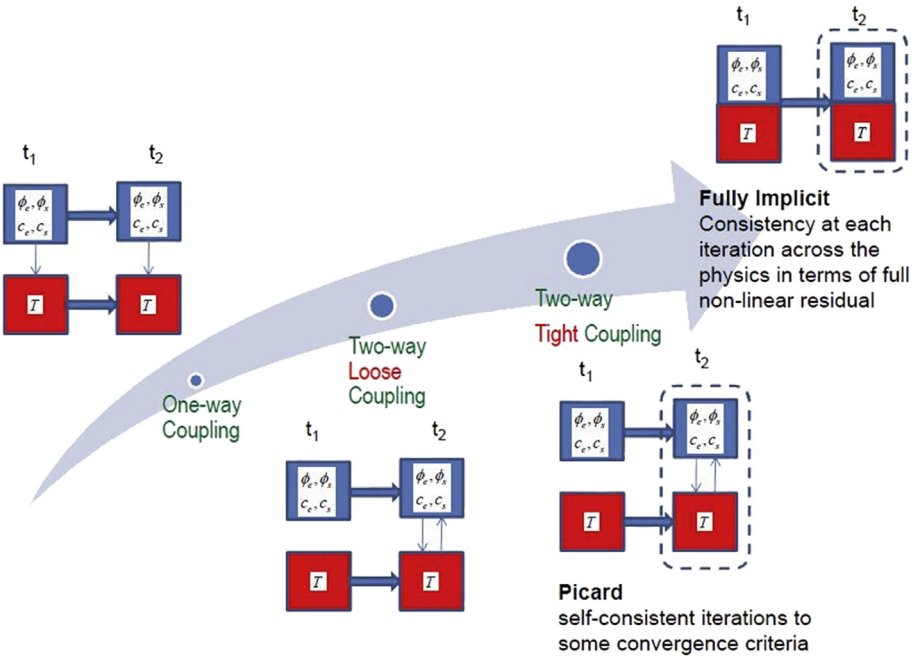

Fig. 5. Coupling scenarios in battery modeling.

material and petroleum derived carbon coke was used as anode. The electrolyte consisted of $LiPF_6$ salt in non-aqueous mixture of ethylene carbonate (EC) and dimethyl carbonate (DMC) in a poly(vinyl difluoride)-hexafluoropropylene (PVDF-HFP) polymer matrix. The coefficients of the equation describing the concentration-dependent conductivity of the electrolyte, as well as the other model parameters (transference numbers, electrode film thicknesses, etc.) were adopted from Ref. [23]. Effective ionic conductivity (k^{eff}) in Eq. (5) follows the effective medium approach as

$$k^{\text{eff}} = \varepsilon^p k_e \tag{13}$$

with $p = 3.3$ and the conductivity of electrolyte represented as a function of the lithium concentration [23]

$$k_e = 4.1253\cdot10^{-4} + 5.007\cdot10^{-3}c_e - 4.7212\cdot10^{-3}c_e^2 + 1.5094\cdot10^{-3}c_e^3 - 1.6018\cdot10^{-4}c_e^4 \tag{14}$$

The effective diffusivity (D_e^{eff}) in Eq. (2) follows the same effective medium law Eq. (13) with the same exponent equal to 3.3. The length and the width of the unrolled cell were 50 cm and 2.4 cm, respectively [29], which equates to 1C discharge current density of 17.5 Ah m^{-2}. The values of the parameters used in the electrochemical model are listed in Table 1. Table 2 lists the parameters used for thermal modeling. The thermal conductivity values for positive and negative electrode materials listed in Table 2 were taken from Ref. [34].

The temperature distribution in the unrolled cell corresponding to two different C-rates is shown in Fig. 3. The temperature shown is at the end of discharge. The time step size (for interaction of data between the components while internally *DualFoil* might take much smaller time steps) sensitivity was tested with different values. It was determined that the difference in maximum temperature prediction between 10 and 20 time steps was 0.3% which indicates good convergence. Cell cooling was simulated by prescribing temperature of 298 K at the top surface. The remaining surfaces are modeled as perfect insulators, zero heat flux or adiabatic [29], which is the default boundary condition for FEM thermal formulation. These conditions would lead to thermal gradient which requires that the cell be divided into 15 zones (segments) along the longitudinal *y*-axis (as the temperature varies in that direction) with *DualFoil* component providing electrochemical state for each zone. For the composition of the cell under consideration and the thermal properties of the components 15 zones distributed along longitudinal *y*-axis of the cell was determined to be sufficient to obtain convergence in results of thermal simulation.

Table 1
Electrochemical (*DualFoil*) modeling parameters.

Parameter	Value
Thickness of negative electrode [m]	128.0×10^{-6}
Thickness of positive electrode [m]	190.0×10^{-6}
Thickness of negative current collector [m]	10.0×10^{-6}
Thickness of positive current collector [m]	15.0×10^{-6}
Initial salt concentration [mol m^{-3}]	2000
Diffusion coefficient in $LiMn_2O_4$ [m^2 s^{-1}]	1.0×10^{-13}
Diffusion coefficient in LiC_6 [m^2 s^{-1}]	3.9×10^{-14}
Volume fraction of electrolyte in positive electrode	0.444
Volume fraction of electrolyte in negative electrode	0.357
Radius of particles in positive electrode [m]	8.5×10^{-6}
Radius of particles in negative electrode [m]	12.5×10^{-6}
Conductivity of positive electrode [S m^{-1}]	3.8
Conductivity of negative electrode [S m^{-1}]	100.0
Cathodic reaction rate constant	3.0×10^{-11}
Anodic reaction rate constant	1.0×10^{-5}
Cation transference number	0.2

Table 2
Parameters used for thermal modeling.

Component	Density (kg m^{-3})	Heat capacity (J kg^{-1} K^{-1})	Thermal conductivity (W m^{-1} K^{-1})
Positive current collector	2700	900	238
Positive electrode	1500	700	5
Negative current collector	8960	385	398
Negative electrode	2500	700	5
Separator	1200	700	1

As can be seen, the discharge at 1C (Fig. 6(a)) and 2C (Fig. 6(b)) causes significant temperature gradients, which are greater at the higher discharge rate. As much as 70 °C maximum temperature can be achieved at the end of discharge at 2C.

The lithium concentration profiles in electrolyte for various discharge rates across the cell sandwich are shown in Fig. 7(a). These are obtained at the end of discharge when the cell potential has dropped to 2 V and one can see severe gradients in the Li^+ concentration due to slow diffusion across the thick cathode. Significant gradients in electrode composition Fig. 7(b) develop with increasing applied discharge rates due to rate of lithium insertion into manganese oxide cathode and compounded by the gradients in Li^+ concentration in the electrolyte. The difference between the maximum and minimum Li content in $LiMn_2O_4$ through the electrode thickness is as much as 4.6% in case of 4C discharge rate.

Next, the current collectors and the electrical model component Eq. (12) were added to the above system to model the NC and PC domains. The electrical component provides the electrical current density solution within the cell sandwich thus providing the heat sources for the thermal component within the NC and PC domains. Fig. 8 depicts the temperature distribution of this unrolled cell with current collectors. It should be mentioned, that while inclusion of electrical model and current collectors results in additional heat sources arising from the ohmic heating, the magnitude of such heating is much smaller than the sources coming from polarization Eq. (9). As can be seen from comparison of Figs. 6 and 8, addition of current collectors results in overall lower temperatures within the cell, due to the heat dissipation through metal current collectors. Compared to the results in Fig. 6 the maximum temperature decreased by 3% and the temperature gradient within the cell longitudinal direction decreased as well. The total time taken to complete a single simulation is around 3 min with a finite element

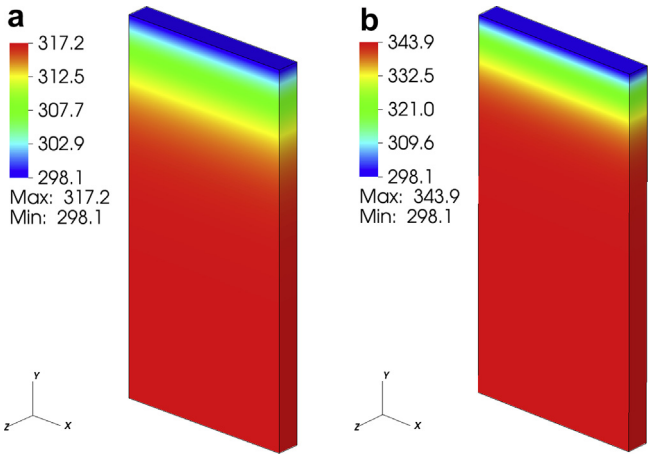

Fig. 6. Temperature distribution (in K) in unrolled cell at the end of discharge at: (a) 1C, (b) 2C (*Not to scale*).

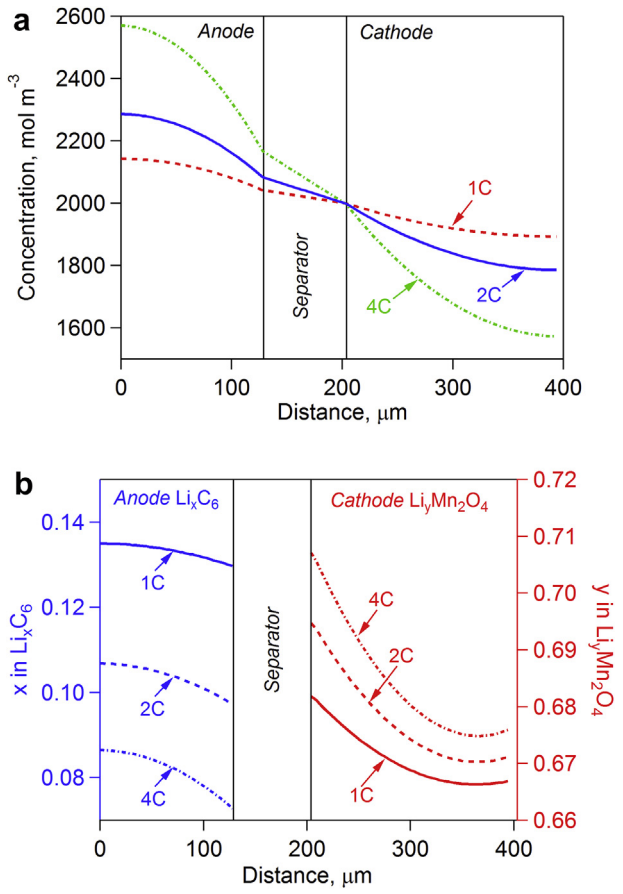

Fig. 7. Effect of discharge rate on (a) lithium concentration in electrolyte, (b) electrode composition.

mesh of 3000 degrees of freedom for both thermal and electrical components.

4.2. Cylindrical cell

In this study, we use the same battery components as in the first study rolled into a cylindrical cell. The cell was 2 cm in diameter and 5 cm long with eight spiral wounds of the sandwich configuration containing the same active materials as in the case of unrolled cell. For this geometry and material composition, the discharge at 1C rate corresponds to current density of 22 Ah m^{-2}. Material constants and parameters listed in Tables 1 and 2 were used in this simulation. Fig. 9 shows the geometry and the finite element mesh used to resolve the geometry of the cylindrical cell including the current collectors. The model has 168 zones that are partitioned into 4 quadrants. Each quadrant has 28 distinct zones representing the cell-sandwich (S domain) and positive (PC) and negative current (NC) collectors. The cutout in Fig. 9 shows the distribution of zones within one quadrant with electrochemical (charge transfer) zones representing cell sandwich shown with different colors. The simulation uses 56 concurrent *DualFoil* simulations for different cell-sandwich zones within the cell. Convective (Robin) boundary condition was applied to the cell surface with the convective heat transfer coefficient equal to 25 W m^{-2} K^{-1} and in this case, the cell casing was not modeled. The results of temperature distribution at the end of 2C discharge are shown in Fig. 10. The maximum temperature occurs at the cell core as expected. The total time required to run this single simulation is approximately 10 min with a finite element mesh of 30,000 degrees of freedom for both thermal and electrical components.

4.3. Pouch cell: experimental validation

In this study, we use all the physics components for modeling the performance characteristics of the pouch cell. The cell under consideration is a 70 mm × 110 mm × 10 mm 4.3 Ah pouch cell manufactured by Farasis Energy, Inc. The experimental discharge profiles of this cell for different C-rates are shown in Fig. 11.

NTG model was chosen to represent the electrochemical component within the framework. The experimentally obtained discharge data (Fig. 11) was used to calculate the variables within the linearized polarization model Eq. (1) and obtain the fitting constants based on the procedure described earlier (Fig. 2). Coefficients for the 6-th order polynomial fits are provided in Table 3.

The resulting functions for the open circuit potential U and the polarization parameter Y are shown in Fig. 12. The coefficient of determination, R^2, for these fits is 0.962 for Y and 0.998 for U. The simulated cell potential as a function of the depth of discharge (θ) is shown in Fig. 12(c) for 1C and 5C applied currents.

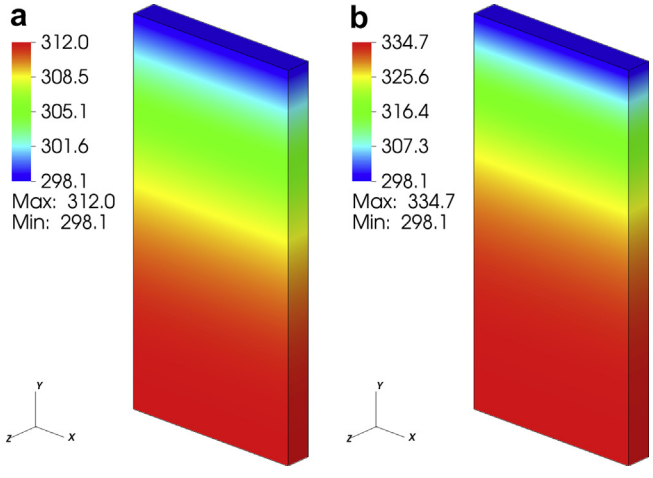

Fig. 8. Temperature distribution (in K) in unrolled cell with consideration of current collectors: (a) end of discharge at 1C; (b) 2C (*Not to scale*).

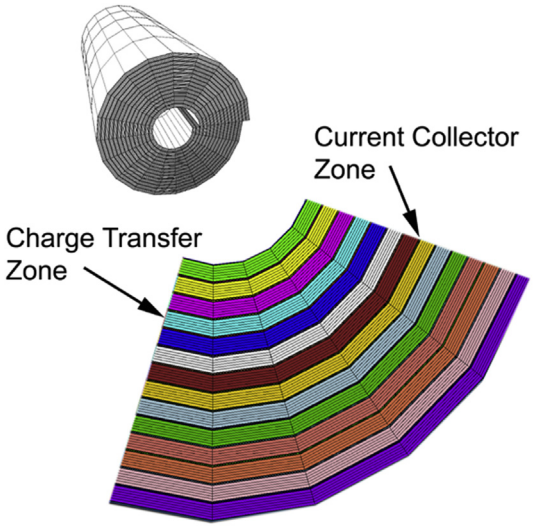

Fig. 9. Finite element mesh and distribution of zones in the cylindrical rolled cell.

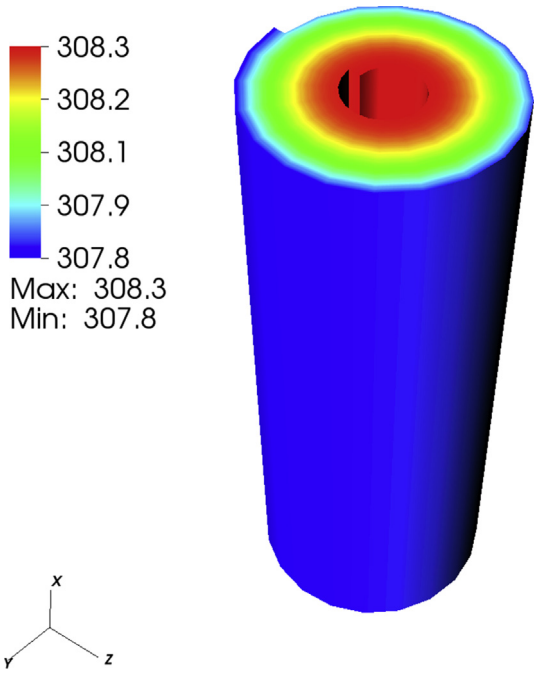

Fig. 10. Temperature distribution in a rolled cylindrical cell subject to 2C discharge current.

The pouch cell in the current study contained 17 cathode and 17 anode layers, therefore the finite element mesh for thermal and electrical analyses needed to be more refined to resolve the current collectors and the cell sandwich. The finite element mesh was divided into 71 corresponding zones for cell sandwich (S domain) and current collectors (NC and NP domains). In addition, two zones were added on the sides of the cell to represent the pouch material (P domain). The cell pouch is coupled to thermal physics only as it does not participate in any electrochemical processes or electrical transport within the cell. The thermal conductivity of the pouch material was estimated based on a three-layer pouch material structure (DNP Inc., Japan) with two isolative layers (Nylon and Polypropylene) sandwiching the aluminum layer in between. Based on the parallel and series formulations for anisotropic thermal conductivity Eq. (10), the conductivity of the pouch in transversal direction was calculated as $k_z = 0.263$ W m^{-1} K^{-1} and in the other two directions as $k_x = k_y = 7.75$ W m^{-1} K^{-1}. Density and heat

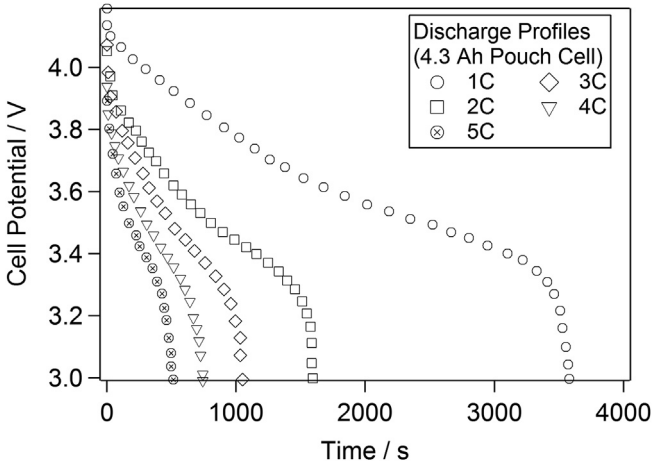

Fig. 11. Experimental discharge curves of the 4.3 Ah Li-ion pouch cell.

Table 3
Coefficients for NTG model (Eq. (1)).

U [V]	Y (S m^{-2})
$a_0 = 4.121$	$b_0 = 3.6433 \times 10^2$
$a_1 = -1.0206$	$b_1 = -2.0629 \times 10^3$
$a_2 = -1.1902$	$b_2 = 1.1248 \times 10^4$
$a_3 = 8.2938$	$b_3 = -2.8978 \times 10^4$
$a_4 = -20.6735$	$b_4 = 4.0999 \times 10^4$
$a_5 = 24.8684$	$b_5 = -3.1353 \times 10^4$
$a_6 = -11.0442$	$b_6 = 9.8589 \times 10^3$

capacity of the pouch material were 1150 kg m^{-3} and 1900 J kg^{-1} K^{-1} respectively. The finite element mesh for the cell is shown in Fig. 13. A cutout in Fig. 13 represents the details of the distribution of the zones within the cell. An idealized weld with zero contact resistance is assumed for joining all the current collectors to the tab leads where a current flux boundary condition is imposed. The simulation uses 34 concurrent NTG model instances for solving the electrochemical potential in each cell sandwich.

The results of temperature distribution at the end of two different discharge rates are shown in Fig. 15. A mixed boundary condition is used on the pouch surfaces for the thermal model to simulate cooling. Typical values of heat transfer coefficient corresponding to free convection with air range from 5 to 25 W m^{-2} K^{-1}. The value for convective heat transfer coefficient is estimated from the temperature measurements of the cell during the rest periods after each discharge (Fig. 14). In the absence of the heat sources and assuming uniform temperature across the cell thickness, the solution of the thermal transport equation has a simple exponential form $T - T_{amb} = \exp(-t/\tau)$ where $\tau = mC_p/h_T A_s$ and h_T is the heat transfer coefficient, m is the mass of the cell, and A_s is the cell surface area. The experimental temperature measurements during cell rest were fitted with this exponential function.

The cooling slope was very consistent between the curves and the average was $\tau_{avg} = 463.02$ s, which corresponds to 15.48 W m^{-2} K^{-1} heat transfer coefficient. For the present numerical study, a convective heat transfer coefficient of 15 W m^{-2} K^{-1} was used in the Robin (mixed) boundary conditions to represent the natural convection cooling of the battery surface. This configuration results in a temperature gradient in the cell's through thickness direction and the maximum temperature at its center. In order to validate the modeling results, thermal measurements were performed on the cell during discharging at different C-rates (Fig. 11). The temperature was measured using an IR camera and the data was obtained at the geometrical center of the cell surface.

A comparison between simulated and experimentally measured temperature is shown in Fig. 16. The markers represent the experimental data and the solid lines correspond to the simulation results. As can be seen the predictions of the temperature values are in a good agreement with the experiment. The maximum error of the temperature prediction using NTG model is below 5% for all of the discharge rates considered. The total time required to run this single simulation is around 6 min with a finite element mesh of 30,000 degrees of freedom for both thermal and electrical components.

5. Discussion

The primary goals of the current report are: a) to demonstrate the flexibility of the new open architecture software computational framework developed within the CAEBAT program and b) to validate the simulation results from the new 3D approach that resolves the current collectors with the experimental data. The framework is

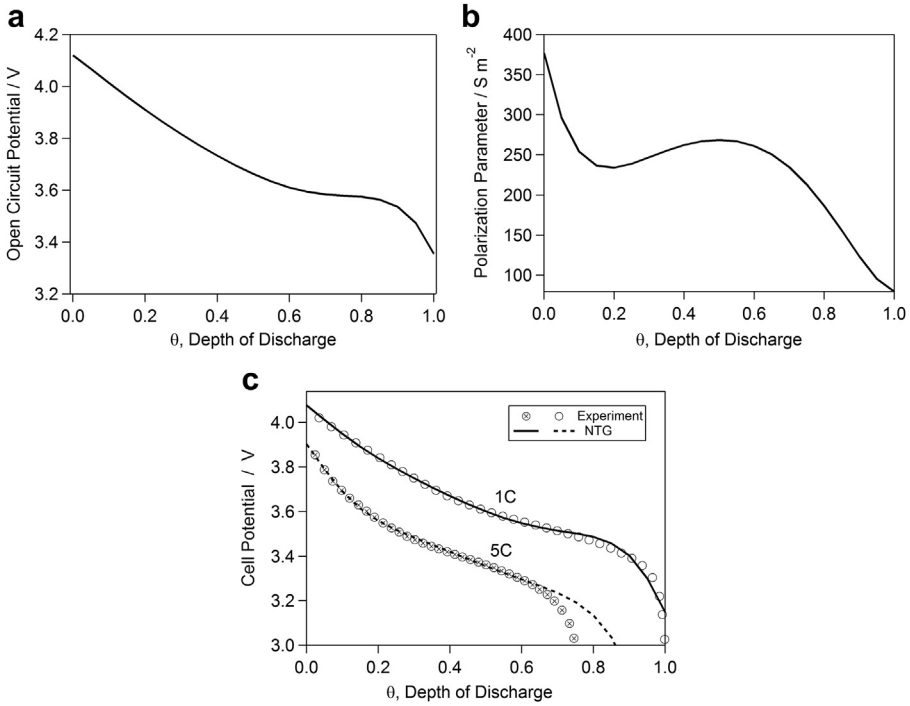

Fig. 12. Parameters used in NTG model: (a) open circuit potential; (b) cell polarization parameter; (c) calculated cell potential as a function of depth of discharge.

designed for coupling different physics for thermal and performance modeling of lithium-ion batteries. The modular structure of the framework, where each physical process is represented by a computer code component provides convenience in switching between the models representing different processes in battery simulation. Indeed, in order to substitute, add, or remove components from the overall model, the end user merely needs to change a few lines in the simulation configuration file.

At the current stage three components have been integrated into the framework representing electrochemistry, thermal and electrical transport. Two-way loose coupling between the components was used in the present simulations (Fig. 5). The exchange of the data between the components is set up in such a way (Fig. 4) that the solution of electrochemical module provides the resistances within the cell which are passed to the electrical module for solution for potential in the battery. The heat sources computed by electrochemical module with inclusion of the ohmic heat from the electrical module are passed to the thermal component to obtain the temperature distribution. In this manner, a true 3D distribution of potential and temperature is obtained as a result of the simulation and as far as we know this is the first implementation of this nature.

As in many instances of mathematical modeling work, determination of material constants and system parameters necessary for conducting a simulation presents a challenging task. In this regard, the *DualFoil* model, being based on the porous electrode theory, requires significant number of material parameters, many of which are not readily available. The model calls for such parameters as Li-ion diffusivities in all of the members constituting the cell sandwich as well as composition volume fractions and specific surface areas of the electrodes. The latter can be estimated [23] by assuming the electrode particles being spherical of equal radius R_s as $a = 3(1-\varepsilon)/R_s$, but this formula invokes determination of electrolyte volume fraction ε which requires porosimetry experiments being conducted on the electrode. This formula was used in the current *DualFoil* calculations with electrolyte volume fractions in the electrodes taken from the literature (Table 1). Finally, the exponent p in the equation for ionic conductivity of electrolyte Eq. (13) is determined from the best fitting the discharge curve data [23]. NTG model on the other hand, while unable to provide details of spatial distribution of variables (e.g., Li concentration in the cell sandwich) requires only availability of the discharge curves at several discharge rates. Being empirical in nature it gives good predictions of the cell electrochemical behavior and since all the parameters are represented as polynomials, the savings in compute time are tremendous. Therefore, this model could be suitable for computations involving large number of concurrent runs of electrochemical component - that is for large systems such as battery modules and packs. The model requires determination of cell conductance (Y) and open circuit potential (U) as functions of the depth of discharge. It should be re-iterated that Y

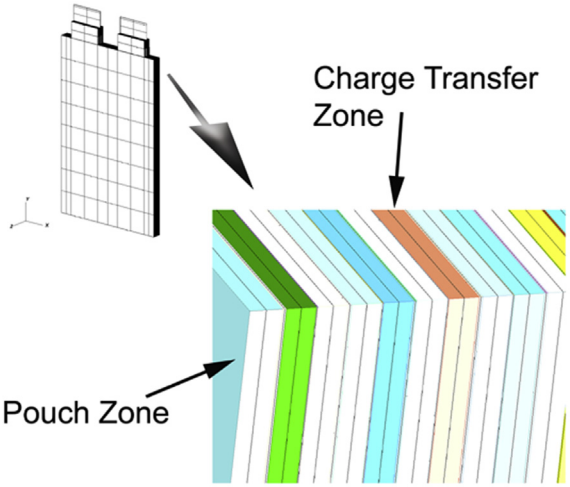

Fig. 13. Finite element mesh and distribution of zones in the pouch cell.

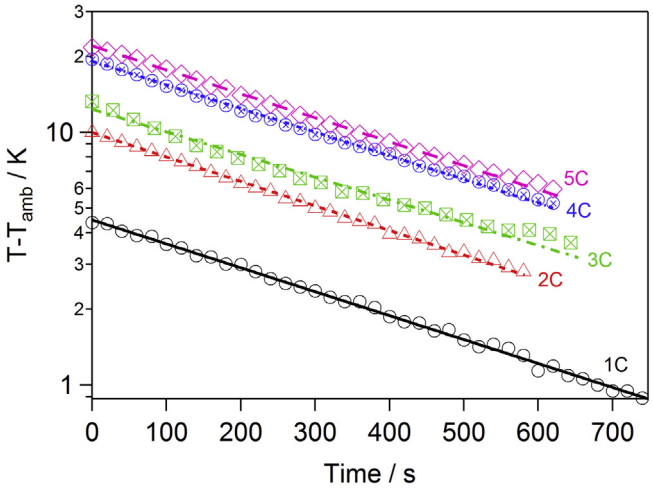

Fig. 14. Temperature drop in the cell during the rest periods after discharge at different rates.

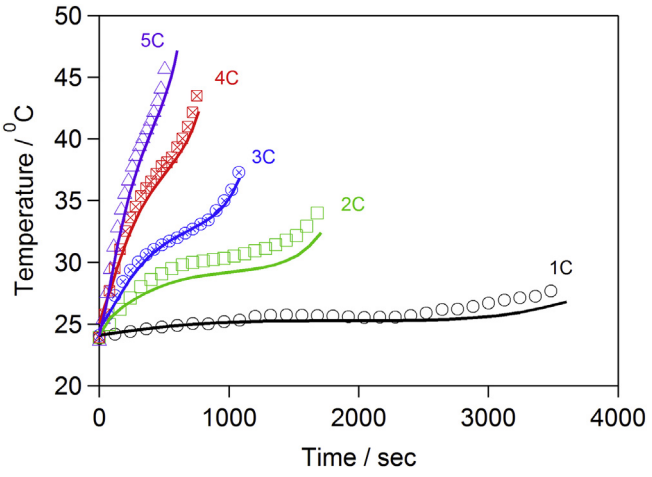

Fig. 16. Comparison between experimentally measured and predicted by modeling temperatures at the pouch cell surface.

is the fundamental electrochemical quantity containing information about electrode polarization resistance as well as resistance of the electrolyte and separator. This parameter can be obtained via rigorous mathematical derivations [35] and in general is a non-linear function of the cell potential. The representation in the NTG model can be considered as a linear approximation to the full polarization curve, derived from the empirical data. While approximate, such treatment yields reasonable predictions, as can be seen in Fig. 16. Since the NTG model describes combined effect of processes occurring in different components of the cell sandwich, addition of the degradation related models which are microstructure-dependant (i.e. stress build-up and fracture, SEI formation, manganese dissolution from $LiMn_2O_4$, etc.) would present a problem, which can be considered as the major drawback of NTG model.

Rigorous treatment of the energy balance in an electrochemical cell requires consideration of heat coming from polarization (irreversible heat loss), entropy change (reversible heat loss), as well as ohmic losses in electrodes, electrolyte and current collectors [27]. A detailed treatment of each of the components and discussion of their influence on the combined heat generation is available in Ref. [29]. Among the terms entering the equation for the heat generation (Eq. (8) and its simplified form Eq. (9)), determination of the reversible heat presents the major challenge as it requires

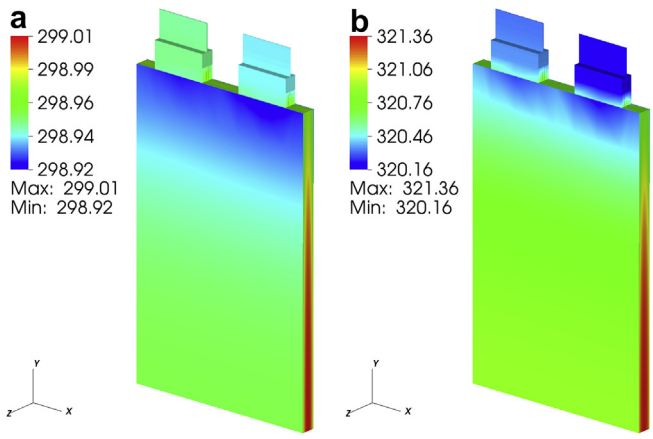

Fig. 15. Temperature distribution in pouch cell at the end of discharge: (a) 1C applied current; (b) 5C applied current.

determination of $\partial U/\partial T$. This quantity is system-specific and is not readily available, which means this term is often excluded from the modeling, especially when simulations are performed at high discharge rates. The importance of the reversible heat obviously diminishes at higher C-rates when high overpotentials dictate the overall heat generation. However, at low and intermediate discharge currents, the entropic heat can constitute as much as 50% of the total heat in some redox systems [36]. Determination of $\partial U/\partial T$ can be based on experimental measurements of the entropy change (ΔS) using electrochemical thermodynamic measurement system (ETMS) technique [37]. The reversible heat source is related to the entropy change as

$$q_{\text{rev}} = -T\frac{\partial U}{\partial T} = T\Delta S\frac{J}{nF} \tag{15}$$

Where, J is the current density, T is temperature, F is the Faraday's constant, and n is the number of electrons transferred during the reaction. For most Li-ion systems $n = 1$. The entropy change is highly system specific, such that $LiCoO_2$ presents much higher entropy change than $LiFePO_4$ cathodes; measurements of the full cell configurations show that the entropy change is highly specific to the electrode pair being used as well [37].

Naturally, the above limitations as well as advantages need to be considered for each simulation set up when the particular models need to be chosen to represent the physical phenomena in the best way. For instance, as was mentioned, thermal modeling of large systems may be coupled to NTG model representing electrochemistry in order to save the compute time. Porous electrode (*DualFoil*) model can be used when the details of distribution of internal variables are of essence, for instance when coupling with degradation models (next step in the current framework development) is desired. The structure of the computational framework presented in the current investigation provides the user with convenience of swapping the models based on such considerations.

6. Conclusions

We presented a new, Open Architecture Software (OAS) computational framework for modeling lithium-ion batteries. The framework integrates electrochemical, thermal, and electrical models for studying battery performance under various discharge rates and other conditions. Several case studies representing different Li-ion cell configurations are presented. The case studies

demonstrate the computational strategy and usage of different models representing electrochemical behavior. Importance of heat dissipation via metal current collectors is shown with the example of unrolled cell, where the temperature can rise up to 70 °C at 2C discharge when current collectors are not included in the model. The validation of the modeling approach is presented by comparison of the predicted transient temperatures in a pouch cell with those experimentally measured at different discharge rates. A good correlation between modeling predictions and experiment was observed.

Acknowledgment

This research at Oak Ridge National Laboratory, managed by UT-Battelle, LLC, for the U.S. Department of Energy under contract DE-AC05-00OR22725, was sponsored by the Vehicle Technologies Program for the Office of Energy Efficiency and Renewable Energy (with David Howell and Brian Cunningham as program managers). The authors would like to acknowledge that the pouch cell for testing was obtained from Dr. Keith Kepler at Farasis Energy Inc. and the experimental data was obtained from Dr. Hsin Wang at the Oak Ridge National Laboratory.

References

[1] E. Karden, S. Ploumen, B. Fricke, T. Miller, K. Snyder, J. Power Sources 168 (1) (2007) 2–11.
[2] K. Somasundaram, E. Birgersson, A.S. Mujumdar, J. Power Sources 203 (2012) 84–96.
[3] N. Nieto, L. Diaz, J. Gastelurrutia, I. Alava, F. Blanco, J.C. Ramos, A. Rivas, J. Electrochem. Soc. 160 (2) (2013) A212–A217.
[4] R.E. Gerver, J.P. Meyers, J. Electrochem. Soc. 158 (7) (2011) A835–A843.
[5] A. Awarke, M. Jaeger, O. Oezdemir, S. Pischinger, Int. J. Energy Res. 37 (6) (2013) 617–630.
[6] J. Gomez, R. Nelson, E.E. Kalu, M.H. Weathersoon, J.P. Zheng, J. Power Sources 196 (10) (2011) 4826–4831.
[7] M. Guo, G.-H. Kim, R.E. White, J. Power Sources (2013), http://dx.doi.org/10.1016/j.jpowsour.2013.03.170.
[8] S. Chacko, Y.M.M. Chung, J. Power Sources 213 (2012) 296–303.
[9] D. Danilov, P.H.L. Notten, Electrochim. Acta 53 (2008) 5569–5578.
[10] J. Christensen, J. Newman, J. Electrochem. Soc. 153 (6) (2006) A1019–A1030.
[11] Y.-T. Cheng, M.W. Verbrugge, J. Appl. Phys. 104 (2008) 083521-1–083521-6.
[12] A.M. Colclasure, R.J. Kee, Electrochim. Acta 55 (28) (2010) 8960–8973.
[13] M. Doyle, T.F. Fuller, J. Newman, J. Electrochem. Soc. 140 (6) (1993) 1526–1533.
[14] M.B. Pinson, M.Z. Bazant, J. Electrochem. Soc. 160 (2) (2013) A243–A250.
[15] Long Cai, Ralph E. White, J. Power Sources 196 (14) (2011) 5985–5989.
[16] Gerardine G. Botte, Venkat R. Subramanian, Ralph E. White, Electrochim. Acta 45 (15) (2000) 2595–2609.
[17] C.Y. Wang, Venkat Srinivasan, J. Power Sources 110 (2) (2002) 364–376.
[18] G.H. Kim, K. Smith, K.J. Lee, S. Santhanagopalan, A. Pesaran, J. Electrochem. Soc. 158 (8) (2011) A955–A969.
[19] J. Newman, W. Tiedemann, J. Electrochem. Soc. 140 (7) (1993) 1961–1968.
[20] H. Gu, J. Electrochem. Soc. 130 (7) (1983) 1459–1464.
[21] U.S. Kim, J. Yi, C.B. Shin, T. Han, S. Park, J. Electrochem. Soc. 158 (5) (2011) A611–A618.
[22] J. Yi, U.S. Kim, C.B. Shin, T. Han, S. Park, J. Electrochem. Soc. 160 (3) (2013) A437–A443.
[23] M. Doyle, J. Newman, J. Electrochem. Soc. 143 (6) (1996) 1890–1903.
[24] T.F. Fuller, M. Doyle, J. Newman, J. Electrochem. Soc. 141 (1) (1994) 1–10.
[25] M. Doyle, J. Newman, J. Electrochem. Soc. 40 (13–14) (1995) 2191–2196.
[26] M. Doyle, T.F. Fuller, J. Newman, Electrochim. Acta 39 (13) (1994) 2073–2081.
[27] D. Bernardi, E. Pawlikowski, J. Newman, J. Electrochem. Soc. 132 (1) (1985) 5–12.
[28] C.R. Pals, J. Newman, J. Electrochem. Soc. 142 (10) (1995) 3274–3281.
[29] V. Srinivasan, C.Y. Wang, J. Electrochem. Soc. 150 (1) (2003) A98–A106.
[30] K. Smith, C.Y. Wang, J. Power Sources 160 (1) (2006) 662–673.
[31] W.R. Elwasif, D.E. Bernholdt, A.G. Shet, S.S. Foley, R. Bramley, D.B. Batchelor, L.A. Berry, in: Proceedings of 2010 18th Euromicro International Conference, 2010, pp. 419–427.
[32] W.R. Elwasif, D.E. Bernholdt, S.S. Foley, A.G. Shet, R. Bramley, in: Proceedings of 9th IEEE/ACS International Conference, 2011, pp. 188–195.
[33] W.R. Elwasif, D.E. Bernholdt, S. Pannala, S. Allu, S.S. Foley, in: Proceedings of IEEE 15th International Conference, 2012, pp. 102–110.
[34] D.R. Baker, M.W. Verbrugge, J. Electrochem. Soc. 146 (7) (1999) 2413–2424.
[35] G. Trost, V. Edwards, J. Newman, in: J.J. Carbury, A. Varma (Eds.), Chemical Reaction and Reactor Engineering, Marcel Dekker, Inc., New York, 1987, p. 923.
[36] J.-S. Hong, H. Maleki, S. Al Hajjaj, L. Redey, J.R. Selman, J. Electrochem. Soc. 145 (5) (1998) 1489–1501.
[37] V.V. Viswanathan, D. Choi, D. Wang, W. Xu, S. Towne, R.E. Williford, J.-G. Zhang, J. Liu, Z. Yang, J. Power Sources 195 (2010) 3720–3729.

Nomenclature

a: specific area
a_i: OCP fitting constants in NTG model
b_i: polarization parameter fitting constants in NTG model
c_e: Li-ion concentration in electrolyte
c_s: Li-ion concentration in solid phase
C_p: heat capacity
D_e^{eff}: effective diffusivity in electrolyte phase
D_s: diffusivity in solid phase
f_A: mean molar activity coefficient of the salt in electrolyte
F: Faraday's constant
h: thickness of the cell
h_T: heat transfer coefficient
i^0: exchange current density
i_e, i: current density in electrolyte and solid phase
j_n: Li-ion flux across the solid–electrolyte interface
J: current density transferred from the negative electrode to the positive electrode
k_i: components of the thermal conductivity
k^{eff}: effective ionic conductivity of electrolyte
q: volumetric heat source
R: universal gas constant
R_s: active material particle radius
r: resistance
t_+^0: lithium transference number
T: temperature
U: open circuit potential (OCP)
V_p: positive electrode potential
V_n: negative electrode potential
α_a: anodic transfer coefficient
α_c: cathodic transfer coefficient
ε: volume fraction of electrolyte in composite electrode
ϕ_e: electrolyte potential
ϕ_s: solid phase potential
η: overpotential
ρ: material density
σ_i: components of electric conductivity
θ: depth of discharge